Article:
Arabansari, S., Davidson, J. orcid.org/0000-0002-6576-3995 and Foster, M. (2022) Fully-integrated planar transformer with a segmental shunt for LLC resonant converters. IEEE Transactions on Industrial Electronics, 69 (9). pp. 9145-9154. ISSN 0278-0046

https://doi.org/10.1109/tie.2021.3116574

Fully-integrated Planar Transformer with a Segmental Shunt for LLC Resonant Converters

Sajad A. Ansari, Jonathan N. Davidson and Martin P. Foster

***Abstract*—This paper presents two topologies which provide high leakage inductance in shunt-inserted integrated magnetic transformers. These differ from conventional designs by replacing the low-permeability magnetic shunt of a planar transformer with high-permeability magnetic shunt segments, separated by many small air gaps. This approach results in a shunt with the same bulk permeability as the conventional design, while using lower cost and readily available magnetic materials such as ferrite. A modelling and design approach which can estimate the leakage and magnetising inductances precisely is provided for each topology. Theoretical analysis is presented and verified using finite-element analysis and experimental implementation. AC resistance analysis for both transformer topologies is also presented. In addition, an LLC resonant converter is built to verify the performance of the proposed fully-integrated magnetic transformers in practice. It is shown that the proposed topologies can integrate all three magnetic components of an isolated LLC resonant converter in a single planar transformer, which reduces the converter's volume and cost.**

***Index Terms*—High-permeability material, integrated magnetic transformer, LLC resonant converter, magnetic shunt.**

I. Introduction

PULSE-WIDTH-MODULATED (PWM) converters, like the boost converter, suffer from the lack of soft-switching capability and thus have high switching losses under high-frequency operation. Losses are limited by constraining the operating frequency, leading to lower power density [1-3]. Even though soft-switching capability can be achieved by adding an auxiliary circuit to the conventional topology of the PWM converters, the auxiliary circuit adds complexity and cost [4-6]. On the other hand, resonant converters provide soft-switching capability inherently. Hence, resonant converters can achieve high efficiency at high switching frequency and are a good choice for the applications in which high power density alongside high efficiency is needed.

The LLC topology is one of the most popular amongst resonant converters and has been used in many applications [7-9]. An isolated LLC resonant converter, shown in Fig.1, uses three magnetic components: a parallel inductor, a series (or resonant) inductor and a transformer. In order to decrease the volume and cost, and increase the efficiency of the LLC resonant converter, all three magnetic elements are usually integrated into a single magnetic component.

There are many methods, which can be used to integrate the magnetic components of the LLC resonant converter. The core of the transformer can be manipulated or an extra core can be added to one of transformer windings to merge either the primary winding or secondary winding with the winding of the series inductor [10-16]. However, this approach requires a new unusual type of core for each design, leading the design process to lower flexibility and higher cost.

Alternatively, a magnetic layer can be added between the layers of the windings to increase leakage inductance [17]. An extra winding can be also inserted into the transformer to merge the series inductance and transformer cores [13, 18]. However, these approaches suffer from higher resistance due to the DC resistance of the additional auxiliary windings and from eddy-currents being induced in all windings. In addition, these approaches cannot provide a high leakage inductance.

The windings of the transformer can be manipulated to achieve a controllable leakage inductance with an interleaved

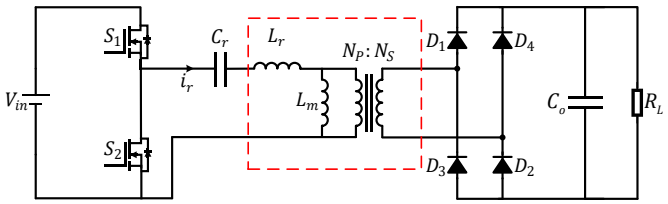

Fig. 1. Topology of the half-bridge LLC resonant converter.

Manuscript received June 11, 2021; revised July 21, 2021; accepted September 18, 2021.

S. A. Ansari, J. N. Davidson and M. P. Foster are with the Department of Electronic and Electrical Engineering, University of Sheffield, Sheffield, S1 3JD, United Kingdom (e-mail: sarabansari1@sheffield.ac.uk; jonathan.davidson@sheffield.ac.uk; m.p.foster@sheffield.ac.uk).

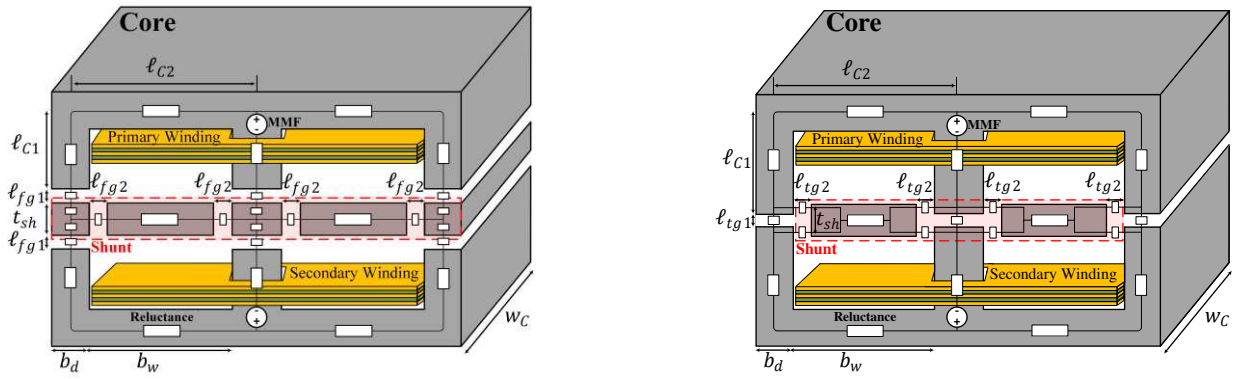

Fig. 2. The proposed segmental shunt-inserted integrated magnetic transformers. (a) Five-segment topology. (b) Two-segment topology.

windings structure which benefits from lower AC resistance [19]. However, in this approach, the winding structure is complicated and the power density is decreased since the windings need to be looped around the outer legs. In addition, the leakage and magnetising inductances are not decoupled and limit each other's values and the flexibility of the design.

Using the estimated leakage inductance as the series inductance and increasing it by inserting air gaps between windings is another method to integrate the magnetic components of an LLC converter [20-24]. However, in this design, the leakage inductance is limited and a high leakage inductance cannot be achieved since it is mainly affected by the geometry of the core and windings.

For converters which take a wide input voltage range, a high series inductance provides the needed high gain for a narrow operating frequency range. Therefore, in recent years, significant effort has been applied to increase the series inductance for integrated LLC converters by increasing the leakage inductance of the integrated magnetic transformer [17, 25]. One way that can provide a high leakage inductance and has an accurate estimation technique for its value is to insert a low-permeability magnetic shunt in the centre of a planar transformer [26, 27]. This method can integrate all three magnetic components of an LLC resonant converter in only a single planar transformer without any auxiliary windings. The relationship between the leakage and magnetising inductances and shunt's characteristics and length of the air gaps for this method is discussed in [26-29]. According to [26-29], the energy stored in the windings and insulation layers is far lower than that stored in the magnetic shunt. In addition, the leakage and magnetising inductances can be controlled for a limited range of leakage inductance and shunt relative permeability by regulating the permeability of the shunt and the length of the air gaps, respectively.

Inserting a single piece low-permeability magnetic shunt in a planar transformer enhances the leakage inductance and makes the estimation of its value more accurate, but this idea suffers from some disadvantages. The magnetic shunt must have a specific and unusually low permeability. Suitable magnetic materials are not often readily available, and when they are, they are frequently expensive. In addition, these low-permeability materials are often found only in limited sizes [26, 30, 31].

To address these issues, two new structures shown in Figs. 2(a) and (b) are proposed. These structures are formed by interleaving highly permeable ferrite with thin plastic spacers to form segmental magnetic shunts. This design approximates the low-permeability material in [27-29]; its permeability is modulated by the ratio of ferrite-to-spacer length. The design is more economical because ferrite is widely available in the market with different sizes and for lower price.

Both of the proposed structures are analysed and their modelling and design guidelines are provided in detail. The theoretical analysis is verified by finite-element analysis (FEA) simulation and experimental results. The AC resistance for the proposed structures is also discussed. Furthermore, an LLC converter is implemented to investigate the performance of the designed fully-integrated magnetic transformers. It is shown that this LLC converter works properly while all of its magnetic components are integrated in the proposed structures.

This study is built on preliminary results [32] presented at the 46th Annual Conference of the IEEE Industrial Electronics Society, 2020, by including a more complete literature review, further theoretical analysis, energy storage analysis and experimental validation.

The paper is organised as follows: the definition of leakage and magnetising inductances and modelling of the proposed integrated magnetic transformers with an inserted-shunt are provided in Section II. In Section III, the calculation of leakage inductance, considering leakage flux going through the window area and windings, is presented. FEA simulation and experimental validation are presented in Section IV. Benefits of the proposed topologies compared to the conventional one-segment shunt topology are discussed in Section V. Finally, a brief conclusion is given in Section VI.

II. Proposed Integrated Magnetic Transformers

The structures of the first and second proposed integrated transformers are shown in Figs. 2(a) and (b), respectively. Subscripts f and t mean five-segment and two-segment, respectively. As shown in Fig. 2, a segmental magnetic shunt is inserted between the magnetic cores of a planar transformer in both topologies. The magnetic shunt of the first and second topologies have five and two segments, respectively. In addition, both the primary and secondary windings are separated by being placed at opposite sides away from the

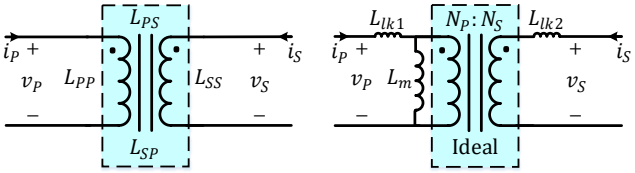

Fig. 3. Coupled inductor models. (a) First model. (b) Second model.

shunt. A lumped parameter magnetic equivalent circuit is superimposed on the transformer geometry to show the locations of the core, shunt and air gap reluctances, and the winding magnetomotive force (MMFs). The modelling of the proposed topologies is discussed in the following.

A. Relationship between magnetising and leakage inductances

A coupled inductor can be modelled according to Fig. 3(a) and the relationship between its voltages and currents may be obtained by (1) [20, 29].

$$\begin{bmatrix} v_P \\ v_S \end{bmatrix} = \begin{bmatrix} L_{PP} & L_{PS} \\ L_{SP} & L_{SS} \end{bmatrix} \frac{\mathrm{d}}{\mathrm{d}t} \begin{bmatrix} i_P \\ i_S \end{bmatrix} \tag{1}$$

where L_{PP} and L_{SS} are primary and secondary self-inductances and L_{PS} and L_{SP} are mutual inductance and i_P and i_S are primary and secondary currents, respectively.

A coupled inductor can be also modelled according to Fig. 3(b) and the relationship between the voltages and currents of this model may be expressed as (2).

$$\begin{bmatrix} v_P \\ v_S \end{bmatrix} = \begin{bmatrix} L_{lk1} + L_m & \frac{N_S}{N_P} L_m \\ \frac{N_S}{N_P} L_m & L_{lk2} + \frac{N_S^2}{N_P^2} L_m \end{bmatrix} \frac{\mathrm{d}}{\mathrm{d}t} \begin{bmatrix} i_P \\ i_S \end{bmatrix} \tag{2}$$

where L_m is the magnetising inductance, N_P and N_S are the primary turns number and secondary turns number and L_{lk1} and L_{lk2} are primary-side and secondary-side leakage inductances, respectively. The magnetising inductance may be obtained by (3).

$$L_m = \frac{N_P}{N_S} L_{PS} \tag{3}$$

The mutual inductance may be defined by (4).

$$L_{PS} = \frac{N_S}{I_P} \phi_{PS} \tag{4}$$

where ϕ_{PS} is the mutual flux produced by the magnetic field of the current in the primary winding that links with the secondary winding and I_P is the RMS of primary current. From (3) and (4), the magnetising inductance is

$$L_m = \frac{N_P}{I_P} \phi_{PS} \tag{5}$$

Hence, to calculate the magnetising inductance of a transformer, the mutual flux of its windings is calculated. The primary self-inductance is

$$L_{PP} = \frac{N_P^2}{R} \tag{6}$$

where R is the core reluctance.

Finally, the total leakage inductance referred to the primary side, L_{lk}, may be calculated by the following equation [20, 29].

$$L_{lk} = 2L_{PP} - 2L_m \tag{7}$$

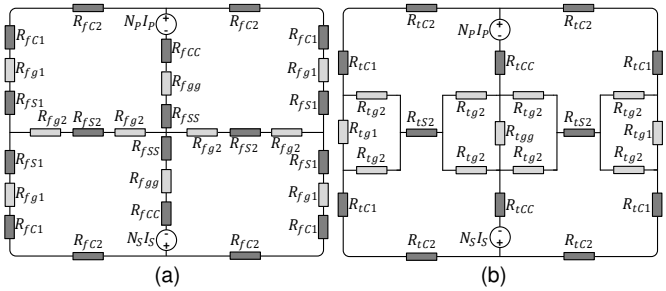

Fig. 4. The reluctance model of the proposed segmental shunt-inserted integrated magnetic transformers. (a) Five-segment topology. (b) Two-segment topology.

B. Five-segment magnetic shunt

The topology of the integrated transformer based on a five-segment magnetic shunt is shown in Fig. 2(a). The magnetic shunt incorporates four equal vertical air gaps with length ℓ_{fg2} (nb. 'f' refers to five segments) to achieve same bulk permeability as the conventional design with the low-permeability shunt. In addition, the horizontal air gaps between the cores and shunt are assumed equal with the length ℓ_{fg1}. The reluctance model of this topology is presented in Fig. 4(a), where R_{fg1}, R_{fgg} and R_{fg2} are air-gap reluctances, R_{fC1}, R_{fC2} and R_{fCC} are core reluctances and R_{fS1}, R_{fS2} and R_{fSS} are shunt reluctances. These are obtained as follows:-

$$R_{fC1} = \frac{\ell_{C1}}{\mu_0 \mu_r b_d w_c} \tag{8}$$

$$R_{fC2} = \frac{\ell_{C2}}{\mu_0 \mu_r b_d w_c} \tag{9}$$

$$R_{fCC} = \frac{\ell_{C1}}{\mu_0 \mu_r A_c} \tag{10}$$

$$R_{fS1} = \frac{t_{sh}}{2\mu_0 \mu_s b_d w_c} \tag{11}$$

$$R_{fS2} = \frac{b_w - 2\ell_{fg2}}{\mu_0 \mu_s t_{sh} w_c} \tag{12}$$

$$R_{fSS} = \frac{t_{sh}}{2\mu_0 \mu_s A_c} \tag{13}$$

$$R_{fg1} = \frac{\ell_{fg1}}{\mu_0 b_d w_c} \tag{14}$$

$$R_{fg2} = \frac{\ell_{fg2}}{\mu_0 t_{sh} w_c} \tag{15}$$

$$R_{fgg} = \frac{\ell_{fg1}}{\mu_0 A_c} \tag{16}$$

where μ_0, μ_r and μ_s are the permeability of the air, core and shunt, respectively. A_C is the core effective cross-sectional area and the definition of other quantities can be found in Fig. 2(a). For brevity, a description for some of the symbols alongside the numerical values used in the FEA simulation and experimental verification is provided later in Table I.

The reluctance model of the topology with a five-segment shunt is shown in Fig. 4(a). Circuit analogue analysis allows mutual flux of the five-segment topology, ϕ_{fPS}, to be calculated as

$$\phi_{fPS} = \frac{2N_P I_P (R_{fS2} + 2R_{fg2})}{R_{fE}(R_{fE} + 2(R_{fS2} + 2R_{fg2}))} \tag{17}$$

where R_{fE} can be defined as

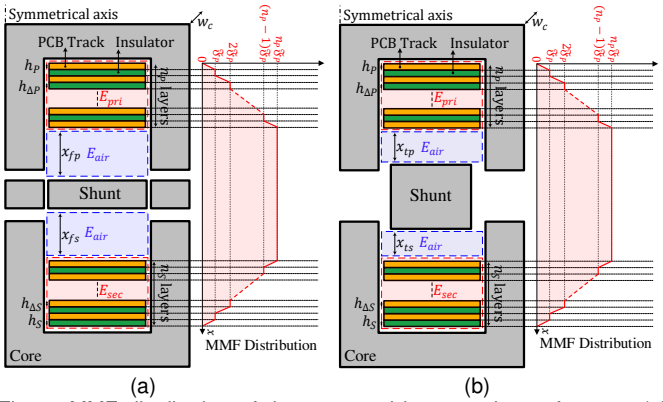

Fig. 5. MMF distribution of the proposed integrated transformers. (a) Five-segment topology. (b) Two-segment topology.

$$R_{fE} = R_{fC1} + R_{fC2} + 2R_{fCC} + R_{fS1} + R_{fg1} + 2R_{fSS} + 2R_{fgg} \quad (18)$$

By substituting (17) into (5), the magnetising inductance of the five-segment topology, L_{fm}, may be calculated using (19).

$$L_{fm} = \frac{2N_P^2(R_{fS2} + 2R_{fg2})}{R_{fE}(R_{fE} + 2(R_{fS2} + 2R_{fg2}))} \quad (19)$$

From (6) and the reluctance model presented in Fig. 4(a), the self-inductance of the primary winding of the five-segment topology, L_{fPP}, may be calculated using (20).

$$L_{fPP} = \frac{2N_P^2(R_{fS2} + 2R_{fg2} + R_{fE})}{R_{fE}(R_{fE} + 2(R_{fS2} + 2R_{fg2}))} \quad (20)$$

Applying (7), (19) and (20), the total leakage inductance caused by the shunt and referred to the primary side of the five-segment topology, $L_{flk-shunt}$, may be calculated using (21).

$$L_{flk-shunt} = \frac{4N_P^2}{R_{fE} + 2(R_{fS2} + 2R_{fg2})} \quad (21)$$

Therefore, from (19) and (21), the magnetising and leakage inductances can be calculated for the design of the transformer.

C. Two-segment magnetic shunt

An alternative approach uses a two-segment shunt and the topology its integrated transformer is shown in Fig. 2(b). This topology benefits from fewer segments which makes the implementation easier. However, in this topology, the entirety of the window area cannot be used for windings and the distance between windings and shunt is reduced, which leads to higher eddy-current losses in the windings as a result of the fringing effect. The magnetic shunt includes two identical segments and there are air gaps between each segment and the cores with length ℓ_{tg2} (nb. 't' refers to two segments). In addition, there are horizontal air gaps between the top and bottom cores with length ℓ_{tg1}. The reluctance model of this topology is presented in Fig. 4(b), where R_{tg1}, R_{tgg} and R_{tg2} are air gap reluctances, R_{tC1}, R_{tC2} and R_{tCC} are core reluctances and R_{tS2} is shunt reluctance and they may be obtained as follows:-

$$R_{tC1} = \frac{\ell_{C1}}{\mu_0\mu_r b_d w_c} \quad (22)$$

$$R_{tC2} = \frac{\ell_{C2}}{\mu_0\mu_r b_d w_c} \quad (23)$$

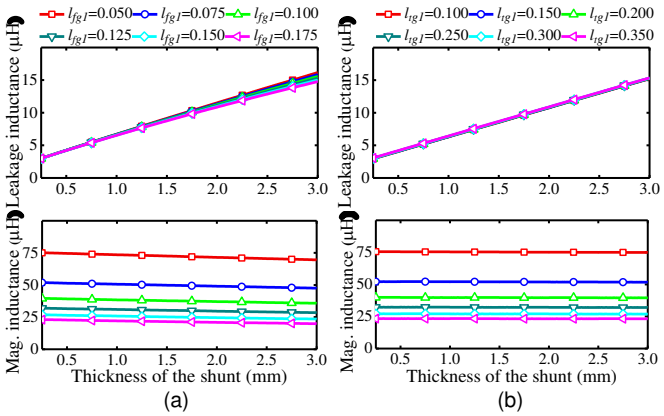

Fig. 6. The calculated leakage and magnetising inductance values. (a) Five-segment topology. (b) Two-segment topology. Core: E32/6/20/R-3F4, ℓ_{fg2}=ℓ_{tg2}=0.5mm, ℓ_{fg1} and ℓ_{tg1} in mm, N_P=10, N_S=2, n_P=5, n_S=2, k_P=2, k_S=1, x_{fp}= x_{fs}=1.5mm, x_{tp}= x_{ts}=0.76mm.

$$R_{tCC} = \frac{\ell_{C1}}{\mu_0\mu_r A_c} \quad (24)$$

$$R_{tS2} = \frac{b_w - 2\ell_{tg2}}{\mu_0\mu_s t_{sh} w_c} \quad (25)$$

$$R_{tg1} = \frac{\ell_{tg1}}{\mu_0 b_d w_c} \quad (26)$$

$$R_{tg2} = \frac{2\ell_{tg2}}{\mu_0 t_{sh} w_c} \quad (27)$$

$$R_{tgg} = \frac{\ell_{tg1}}{\mu_0 A_c} \quad (28)$$

According to the reluctance model of the topology with a two-segment shunt presented in Fig. 4(b), the mutual flux of the two-segment topology, ϕ_{tPS}, may be calculated using (29).

$$\phi_{tPS} = \frac{2N_P I_P(R_{tS2} + R_A + R_B)}{R_{tE}(R_{tE} + 2(R_{tS2} + R_A + R_B))} \quad (29)$$

where R_{tE} can be defined as

$$R_{tE} = R_{tC1} + R_{tC2} + 2R_{tCC} + R_C + R_D \quad (30)$$

and R_A, R_B, R_C and R_D are defined as

$$R_A = \frac{R_{tg2}^2}{R_{tg1} + 2R_{tg2}} \quad (31)$$

$$R_B = \frac{R_{tg2}^2}{2R_{tgg} + 2R_{tg2}} \quad (32)$$

$$R_C = \frac{R_{tg1}R_{tg2}}{R_{tg1} + 2R_{tg2}} \quad (33)$$

$$R_D = \frac{2R_{tgg}R_{tg2}}{2R_{tgg} + 2R_{tg2}} \quad (34)$$

By substituting (5) into (29), the magnetising inductance of the two-segment topology, L_{tm}, is

$$L_{tm} = \frac{2N_P^2(R_{tS2} + R_A + R_B)}{R_{tE}(R_{tE} + 2(R_{tS2} + R_A + R_B))} \quad (35)$$

From (6) and the reluctance model presented in Fig. 4(b), the self-inductance of the primary winding of the two-segment topology, L_{tPP}, is

$$L_{tPP} = \frac{2N_P^2(R_{tS2} + R_A + R_B + R_{tE})}{R_{tE}(R_{tE} + 2(R_{tS2} + R_A + R_B))} \quad (36)$$

From (7), (35) and (36), the leakage inductance caused by the shunt and referred to the primary of the two-segment topology is

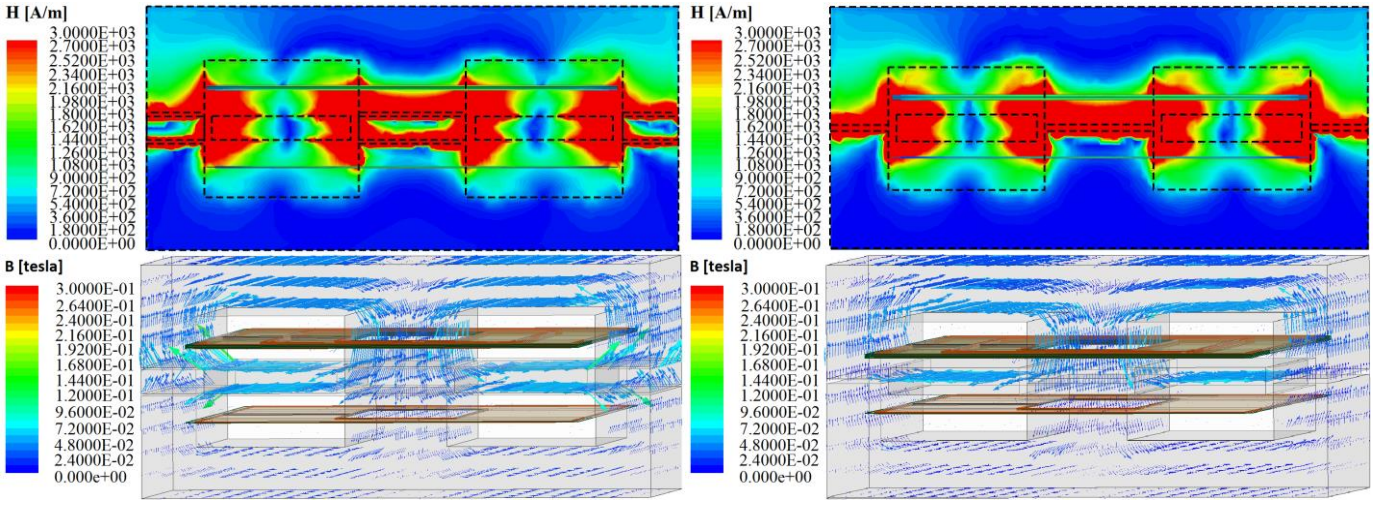

Fig. 7. Magnetic field intensity and magnetic flux density vectors. (a) Five-segment topology. (b) Two-segment topology. E32/6/20/R-3F4.

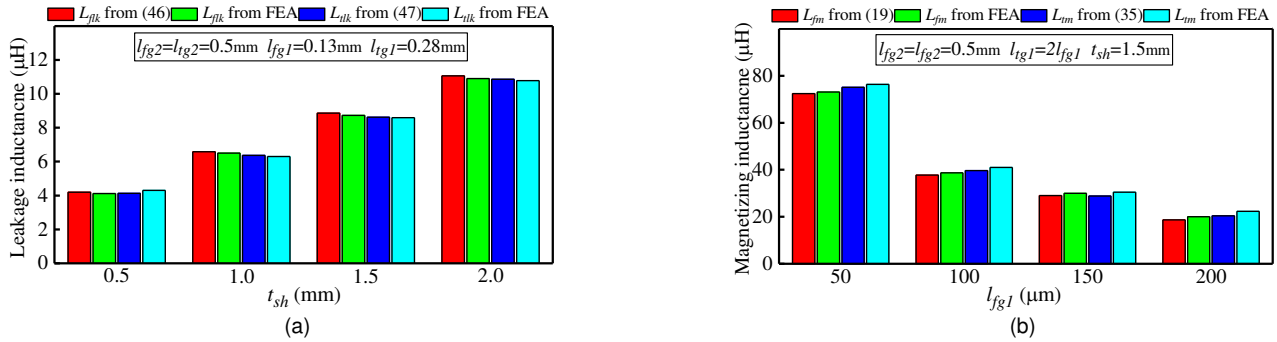

Fig. 8. Modelling verification by simulation results. (a) Leakage inductance. (b) Magnetising inductance.

$$L_{tlk-shunt} = \frac{4N_P^2}{R_{tE} + 2(R_{tS2} + R_A + R_B)} \tag{37}$$

Therefore, from (35) and (37), the magnetising and leakage inductances can be calculated.

III. Leakage Inductance Caused by Window Area and Windings

Ansari et al [32] found that the shunt is responsible for most of the leakage inductance. However, the total energy stored in the leakage inductance includes the energy stored in the window area and the primary and secondary windings too. Careful calculation of the total leakage inductance is thus needed for accurate modelling of the proposed topologies.

The leakage inductance, L_{lk}, may be obtained by (38).

$$E = \frac{1}{2}\iiint_V BH\, dV = \frac{1}{2}L_{lk}I_P^2 \tag{38}$$

where V is the total volume with a cross-section consisting of the window area and the shunt, B is the flux density and H is the magnetic field intensity. The MMF of each layer of the primary winding, $\mathfrak{F}_P$, may be obtained from (39), where k_p is the number of turns in each layer of the primary winding.

$$\mathfrak{F}_P = k_P I_P \tag{39}$$

If n_P and n_S are defined as the number of layers of the primary and secondary windings, respectively, the MMF within the window area, $\mathfrak{F}_{air}$, is $n_P\mathfrak{F}_P$ and the magnetic field intensity

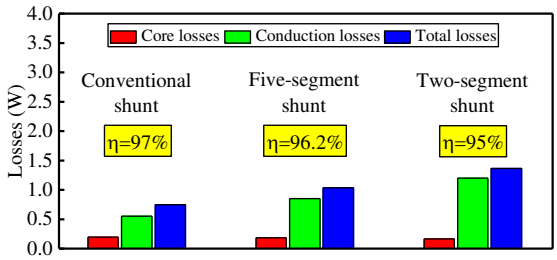

Fig. 9. Loss distribution of different topologies for output power of 25W.

within the air area, H_{air}, may be obtained by the following equation.

$$H_{air} = \frac{n_P\mathfrak{F}_P}{b_w} \tag{40}$$

In addition, from (38), the leakage energy stored in the air, E_{air}, (the area of E_{air} is shown in Fig. 5) may be obtained as follows:-

$$E_{air} = \frac{1}{2}\mu_0 w_c b_w \int H^2 \mathrm{d}x \tag{41}$$

From (40) and (41), the total leakage energy stored in the air gaps of the five-segment (E_{fair}) and two-segment topologies (E_{tair}) may be obtained by (42) and (43), respectively.

$$E_{fair} = 2\frac{1}{2}\mu_0 w_c \frac{n_P^2 k_P^2 I_P^2}{b_w}\left(x_{fp} + x_{fs}\right) \tag{42}$$

$$E_{tair} = 2\frac{1}{2}\mu_0 w_c \frac{n_P^2 k_P^2 I_P^2}{b_w}\left(x_{tp} + x_{ts}\right) \tag{43}$$

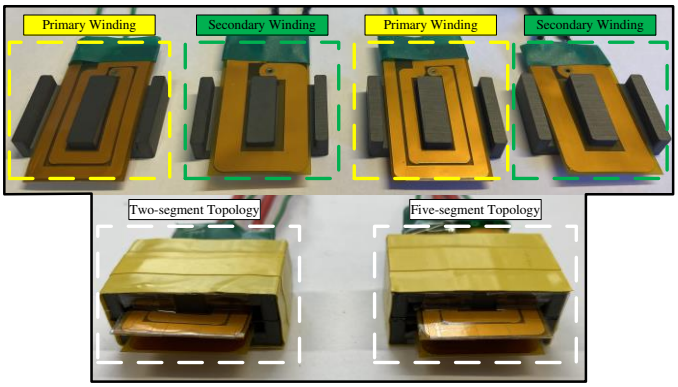

Fig. 10. Prototypes of the proposed topologies. Core: E32/6/20/R-3F4.

TABLE I
PROPOSED STRUCTURES' SPECIFICATION

Symbol	Parameter	value
N_P	Primary turns	10
N_S	Secondary turns	2
k_P	Turns per layer in primary	2
k_S	Turns per layer in secondary	1
n_P	Number of primary layers	5
n_S	Number of secondary layers	2
h_P, h_S	Primary and secondary conduction thickness	35 μm
$h_{\Delta P}$, $h_{\Delta S}$	Primary and secondary insulation thickness	30 μm
w_{PT}	Primary PCB trace wideness	3.1 mm
w_{ST}	Secondary PCB trace wideness	5.7 mm
t_{sh}	Shunt thickness	1.5 mm
ℓ_{fg1}	Five-segment topology horizontal air gap	0.13 mm
ℓ_{tg1}	Two-segment topology horizontal air gap	0.28 mm
ℓ_{fg2}	Five-segment topology vertical air gap	0.5 mm
ℓ_{tg2}	Two-segment topology vertical air gap	0.5 mm
x_{fp}, x_{fs}	Distance between primary and secondary windings and shunt for five-segment topology	1.5 mm 1.5 mm
x_{tp}, x_{ts}	Distance between primary and secondary windings and shunt for two-segment topology	0.76 mm 0.76 mm

where x_{fp} and x_{fs} are the distances between the primary and secondary windings and the shunt for the five-segment topology shown in Fig. 5(a), respectively. x_{tp} and x_{ts} are the distances between the primary and secondary windings and the shunt for the two-segment topology shown in Fig. 5(b), respectively.

The leakage energy stored in the primary and secondary windings, which is the energy stored in the PCB layers of the planar transformer, can be obtained according to the MMF distribution presented in Fig. 5 [22, 27, 28]. Ouyang et al [22] showed that it may be calculated as follows for primary and secondary:-

$$E_{pri} = \frac{1}{6}\mu_0 \frac{w_c}{b_w} k_P^2 [h_{\Delta P}(2n_P^3 - 3n_P^2 + n_P) + 2h_P n_P^3] I_P^2 \quad (44)$$

$$E_{sec} = \frac{1}{6}\mu_0 \frac{w_c}{b_w} k_S^2 [h_{\Delta S}(2n_S^3 - 3n_S^2 + n_S) + 2h_S n_S^3] I_S^2 \quad (45)$$

In (44) and (45), the thickness of the PCB layers of the primary and secondary windings are shown by h_P and h_S, respectively, and the thickness of insulation layers of the primary and secondary windings are shown by $h_{\Delta P}$ and $h_{\Delta S}$, respectively. From (21), (37), (38) and (42)-(45), the total leakage inductance of the five-segment and two-segment topologies may be obtained by (46) and (47), respectively.

$$L_{flk} = 2\mu_0 w_c \frac{N_P^2}{b_w}(x_{fp} + x_{fs}) + \frac{4N_P^2}{R_{fE} + 2(R_{fS2} + 2R_{fg2})} + \frac{1}{3}\mu_0 \frac{w_c}{b_w} k_P^2 n_P^2 \sum_{i=P,S} \left[h_{\Delta i}\left(2n_i - 3 + \frac{1}{n_i}\right) + 2h_i n_i \right] \quad (46)$$

$$L_{tlk} = 2\mu_0 w_c \frac{N_P^2}{b_w}(x_{tp} + x_{ts}) + \frac{4N_P^2}{R_{tE} + 2(R_{tS2} + R_A + R_B)} + \frac{1}{3}\mu_0 \frac{w_c}{b_w} k_P^2 n_P^2 \sum_{i=P,S} \left[h_{\Delta i}\left(2n_i - 3 + \frac{1}{n_i}\right) + 2h_i n_i \right] \quad (47)$$

The calculated leakage and magnetising inductances for the five-segment and two-segment topologies are shown in Figs. 6(a) and (b), respectively. It is clear that the magnetising and leakage inductances are mainly influenced by the horizontal air gaps (ℓ_{fg1} or ℓ_{tg1}) and the thickness of the shunt, respectively. Hence, the leakage and magnetising inductances are sufficiently decoupled from each other in the proposed topologies and can be regulated separately by the thickness of the shunt and the length of the horizontal air gap, respectively.

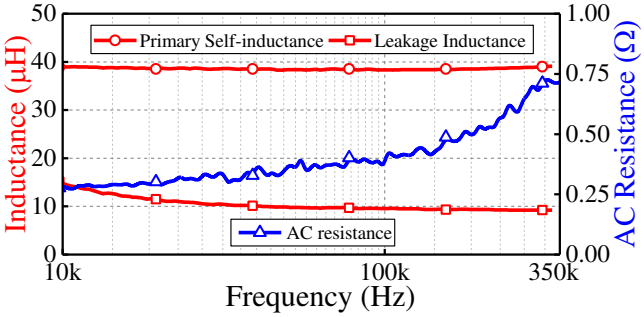

(a)

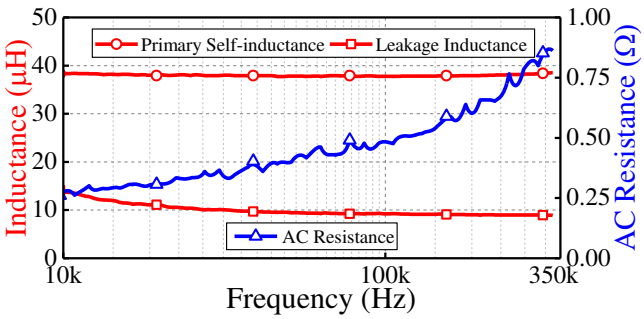

(b)

Fig. 11. Primary self-inductance and leakage inductance and AC resistance versus frequency. (a) Five-segment topology. (b) Two-segment topology.

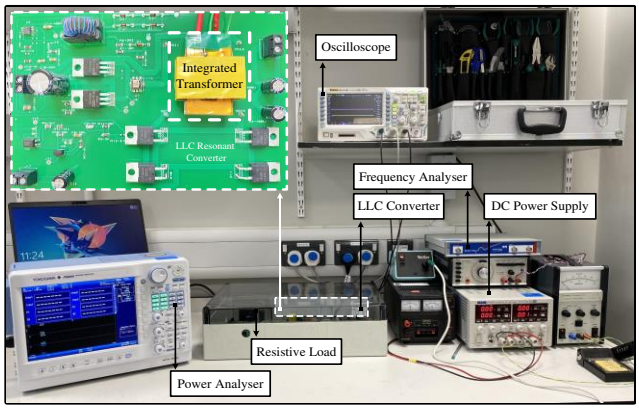

Fig. 12. Prototypes of the implemented LLC resonant converter.

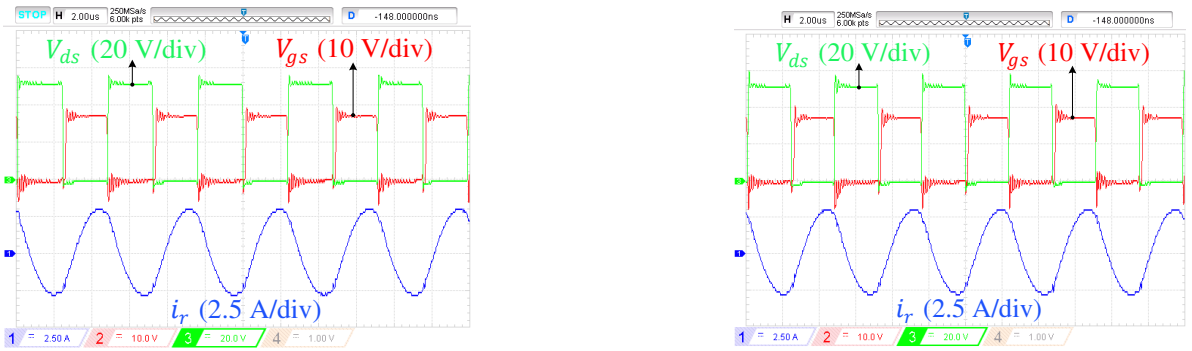

(a) (b)

Fig. 13. Experimental results of the implemented LLC converter. (a) Five-segment topology. (b) Two-segment topology. V_{ds} is drain to source voltage, V_{gs} is gate to source voltage and i_r is the resonant current (primary current of the transformer).

TABLE II
VOLUME COMPARISON BETWEEN DIFFERENT TOPOLOGIES

Topology	t_{sh} (mm)	μ_s	ℓ_{fg1}, ℓ_{tg1} (mm)	ℓ_{fg2}, ℓ_{tg2} (mm)
[29]	1.5	9.5	0.052	-
[29]	1.4	10	0.06	-
5-segment	1.5	800	0.13	0.48
5-segment	1.4	800	0.13	0.45
2-segment	1.5	800	0.28	0.48
2-segment	1.4	800	0.28	0.45

TABLE III
PARAMETERS OF THE IMPLEMENTED TRANSFORMERS

Topology	SYMBOL	Modeling	Simulation	Measurement
Five-segment	L_{fm}	29.08 µH	30.1 µH	29.6 µH
	L_{flk}	8.86 µH	8.72 µH	9.23 µH
Two-segment	L_{tm}	28.81 µH	30.4 µH	28.95 µH
	L_{tlk}	8.61 µH	8.59 µH	8.95 µH

IV. FEA SIMULATION AND EXPERIMENTAL VERIFICATION

Simulation and experimental verification for both topologies with specification presented in Table I (designed according to the Sections II and III) are provided in this section in order to confirm the modelling of the proposed topologies. Rather than design a converter to fit the transformer, the transformer is designed for a typical LLC converter with specification shown later in Table IV.

A. FEA simulation

The magnetic field intensity and flux density vectors for the five-segment and two-segment topologies when the primary winding is excited and a resistor is connected across the secondary winding are presented in Figs. 7(a) and (b), respectively. From Fig. 7, it is clear that the leakage inductance is mainly caused by the shunt since the magnetic field intensity and flux density vectors are higher in the shunt air gaps than window area and windings. The leakage and magnetising inductances versus thickness of the shunt and horizontal air gaps (ℓ_{fg1} and ℓ_{tg1}) calculated from (19), (35), (46) and (47) and obtained by FEA simulation for the five-segment and two-segment topologies are presented in Figs. 8(a) and (b), respectively. As shown, there is only a small discrepancy between the theoretical and simulation results, which verifies the modelling of the proposed topologies.

The loss distribution of the proposed topologies and the conventional one-segment shunt topology obtained by FEA is shown in Fig. 9. It can be seen that the two-segment topology has higher conduction losses compared to the five-segment topology and the reason is explained later. Therefore, even though the two-segment shunt topology benefits from easier manufacturing and smaller volume, it suffers from higher losses. Both proposed topologies have slightly higher conduction losses compared to the conventional single low-permeability shunt topology. This is because a high-permeability shunt with air gaps suffers from higher fringing than a solid low-permeability shunt, leading to higher AC resistance. It should be noted that Sullivan et al [30] have suggested a quasi-distributed gap technique which addresses the issue and could be incorporated into the proposal.

In Table II, the volumes of the proposed topologies and the conventional topology with a low-permeability shunt for the same specifications are provided. As shown, the two-segment topology provides the lowest volume even though it suffers from lowest efficiency. In addition, the proposed topologies can provide the same specification with a range of designs for the shunt (which can be optimized as needed). However, the shunt in the conventional topology cannot be changed for a particular specification unless the permeability of the shunt itself changes. Therefore, not only can the proposed topologies provide a higher power density but they also benefit from increased flexibility in design.

B. Experimental verification

To confirm the theoretical analysis and simulation results, the two- and five-segment topologies are built for the specification presented in Table I and their prototypes are shown in Fig. 10. The measured leakage and magnetising inductances of both topologies at 200 kHz, measured by frequency analyser Omicron Bode 100, are presented in Table III. The measured values are very close to the values obtained by modelling and simulation results. In addition, the primary self- and leakage inductance, and the AC resistance versus frequency for the five-segment and two-segment topologies are shown in Figs. 11(a) and (b), respectively. As shown, the AC resistance of the two-segment topology is higher than the five-segment topology and therefore it has a lower efficiency. Proximity of the gap to the windings in the two-segment topology leads to higher fringing

TABLE IV
THE IMPLEMENTED LLC CONVERTER'S SPECIFICATION

Symbol	Parameter	value
$N_P: N_S$	Turns ratio	10:2
L_m	Magnetising inductance	29 µH
L_r	Resonant (series) inductance	9 µH
C_r	Resonant capacitance	39 nF
V_{in}	Input voltage	45-55 V
V_{out}	Output voltage	5 V
P_{out}	Output power	25 W
f_s	Switching frequency	200-350 kHz
S	Switches	IRF530N
D	Rectifier diodes	12CTQ045

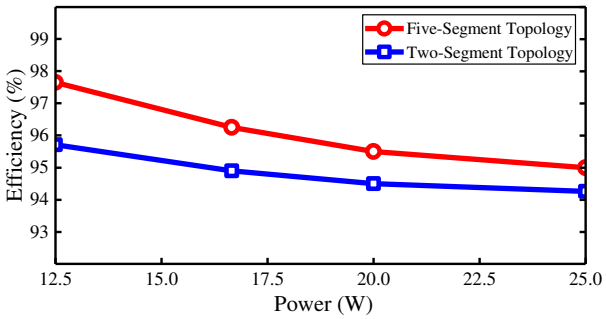

Fig. 14. Efficiency of the LLC converter (excluding the rectifier) at different load conditions.

which explains the reason of this discrepancy.

To verify the performance of the proposed integrated transformers in practice, an LLC converter is implemented and shown in Fig. 12. The LLC converter has been designed according to the procedure outlined in [33] and its specification is shown in Table IV. In this design, the series and parallel inductors are integrated into the transformer. The waveforms of the converter operating at a 210 kHz switching frequency using five-segment and two-segment topologies are shown in Figs. 13(a) and (b), respectively. It can be seen that the switches are turned on at zero voltage (ZVS) because the drain-source voltage drops to zero and then the gate turns ON immediately.

The efficiency of the converter for both topologies is shown in Fig. 14. For this figure, the effect of the asynchronous rectifier is excluded because it is the dominant loss mechanism. It can be seen that, since the two-segment topology has higher AC resistance, it suffers from lower efficiency compared to the five-segment topology. However, it benefits from easier manufacture since it needs only two segments and has smaller volume.

The higher number of segments leads the manufacturing to difficulty and higher cost, but it improves the efficiency of the transformer because of lower fringing. For odd-numbered segments, a five-segment shunt is considered in this work since the reluctance modelling of the topology is very similar to the topology presented in [29]. The even-numbered shunts (for example two) provide a higher power density since the window area is occupied for the shunt. However, even-numbered shunts suffer from higher losses because of fringing effect. Higher odd- and even-numbered segments could have been considered for the proposed topologies to improve the efficiency but it would come with the penalty of more complicated manufacturing and higher cost.

It should also be noted that the application of the proposed topologies is not limited only to the LLC converter and can also be extended to other converters viz phase-shifted full-bridge converters and dual-active bridge converters.

V. DISCUSSION

A high-permeability segmental magnetic shunt technique slightly decreases the efficiency of the transformer; thus, a fair question is whether using the proposed high-permeability segmental shunts is a suitable alternative to using the conventional low-permeability single shunt approach. Hence, the advantages of the proposed topologies are discussed below.

The natural permeability of soft ferrites is a high value. For a particular chemical composition, there is only one permeability and it is therefore easily made available in a range of geometries and sizes. This differs from low-permeability materials whose permeability must be artificially reduced to meet the particular requirement of an application. For these reasons, high-permeability shunts are generally both cheaper and more widely available than low-permeability shunts.

Low-permeability materials are also available for only a limited range of permeabilities, which makes the design of the integrated transformer less flexible. On the other hand, because the same bulk permeability as the conventional one-segment shunt is approximated by vertical air gaps in the proposed topologies, the transformer can be designed with a higher flexibility. In other words, changing the air gaps in a segmental shunt is far easier than the changing the permeability of a non-segmental shunt.

In the proposed topologies, the magnetising and leakage inductances are decoupled in the design process, leading to higher flexibility in design. This is in contrast to the low-permeability single shunt topology where the leakage and magnetizing inductances are only decoupled for a limited range.

The efficiency difference between the five-segment topology and conventional topology is 0.8 percentage points, which is negligible. In addition, even though the two-segment topology has lower efficiency compared to the conventional one (2 percentage points – see Fig. 9), it provides higher power density (10% more as presented in Table II).

In addition, it has been already shown in the literature [30, 31] that using distributed air gaps in a core is better than using low-permeability materials due to the limitations of the low-permeability materials. This distribution air gap method could be extended to be used in the proposed topologies to address the issue of lower efficiency.

The reduced costs from using standard high-permeability materials are likely to be reduced (although not eliminated) for very large production runs. However, there are many small-scale manufacturers with production runs of hundreds to thousands of items for whom a specific magnetic shunt is prohibitively expensive. These manufacturers can still benefit from planar transformers with shunts to achieve high efficiency, but using materials they can access quickly and at commercially viable costs. While less important, availability for prototyping is also a consideration, especially since the proposal allows for

rapid reconfiguration using off-the-shelf materials.

VI. Conclusion

Two new structures for the shunt-inserted integrated planar transformers have been presented in this paper. These structures benefit from a segmental magnetic shunt based on widely-available high-permeability materials which can be found in different sizes and at lower price. The analysis and modelling of both structures, considering the leakage flux going through the shunt, window area and windings, are presented. The leakage and magnetising inductances are decoupled from each other in the proposed topologies and can be designed separately by the thickness of the shunt and the length of the horizontal air gap, respectively. FEA simulation and experimental verification are provided, and they show a good agreement with theoretical predictions. It is shown that while the efficiency of the proposed topologies is slightly less than the conventional topology with low-permeability materials, the power density is enhanced about 10%. In addition, an LLC resonant converter is implemented to prove the performance of the proposed integrated transformers in practice. The prototype shows that both topologies can integrate all three magnetic components of an LLC converter in a single planar transformer as the converter operates properly and its switches are switched at ZVS. The effciency of the LLC converter (excluding the rectifier) with propsoed transformers are measured. According to the measured values, the efficiency of the five-segment topology is 1 percentage points more than two-segment topology even though its power density is about 11% less than two-segment topology. Finally, the advantages of the proposed topologies compared to the conventional topology are discussed to show they can be a suitable alternative for the conventional topology.

References

[1] S. A. Ansari and J. S. Moghani, "A Novel High Voltage Gain Noncoupled Inductor SEPIC Converter," *IEEE Transactions on Industrial Electronics,* vol. 66, no. 9, pp. 7099-7108, 2018.

[2] A. Mirzaee, S. Arab Ansari, and J. Shokrollahi Moghani, "Single switch quadratic boost converter with continuous input current for high voltage applications," *International Journal of Circuit Theory and Applications,* vol. 48, no. 4, pp. 587-602, 2020.

[3] A. Mizani, S. A. Ansari, A. Shoulaie, J. N. Davidson, and M. P. Foster, "Single-active switch high-voltage gain DC–DC converter using a non-coupled inductor," *IET Power Electronics,* 2021.

[4] S. A. Ansari and J. S. Moghani, "Soft switching flyback inverter for photovoltaic AC module applications," *IET Renewable Power Generation,* vol. 13, no. 13, pp. 2347-2355, 2019.

[5] S. A. Ansari, J. N. Davidson, and M. P. Foster, "Evaluation of silicon MOSFETs and GaN HEMTs in soft-switched and hard-switched DC-DC boost converters for domestic PV applications," *IET Power Electronics,* 2021.

[6] S. Arab Ansari, J. S. Moghani, and M. Mohammadi, "Analysis and implementation of a new zero current switching flyback inverter," *International Journal of Circuit Theory and Applications,* vol. 47, no. 1, pp. 103-132, 2019.

[7] Y. Wei, Q. Luo, and A. Mantooth, "Overview of modulation strategies for LLC resonant converter," *IEEE Transactions on Power Electronics,* vol. 35, no. 10, pp. 10423-10443, 2020.

[8] Z. Fang, Z. Huang, H. Jing, and F. Liu, "Hybrid mode-hopping modulation for LLC resonant converter achieving high efficiency and linear behaviour," *IET Power Electronics,* vol. 13, no. 6, pp. 1153-1162, 2020.

[9] C. W. Tsang, M. P. Foster, D. A. Stone, and D. T. Gladwin, "Analysis and design of LLC resonant converters with capacitor–diode clamp current limiting," *IEEE Transactions on Power Electronics,* vol. 30, no. 3, pp. 1345-1355, 2014.

[10] S. Stegen and J. Lu, "Structure comparison of high-frequency planar power integrated magnetic circuits," *IEEE transactions on magnetics,* vol. 47, no. 10, pp. 4425-4428, 2011.

[11] A. Kats, G. Ivensky, and S. Ben-Yaakov, "Application of integrated magnetics in resonant converters," in *Proceedings of APEC 97-Applied Power Electronics Conference*, 1997, vol. 2: IEEE, pp. 925-930.

[12] Y. Liu, H. G. Wu, J. Zou, Y. Tai, and Z. Ge, "CLL Resonant Converter with Secondary Side Resonant Inductor and Integrated Magnetics," *IEEE Transactions on Power Electronics,* 2021.

[13] J. Wang *et al.*, "Design of Integrated Magnetic Transformer for High Frequency LLC Converter," in *2020 4th International Conference on HVDC (HVDC)*, 2020: IEEE, pp. 986-991.

[14] R. Muhammad, S. Kim, C. Suk, S. Choi, B. Yu, and S. Park, "Integrated Planar Transformer Design of 3-kW Auxiliary Power Module for Electric Vehicles," in *2020 IEEE Energy Conversion Congress and Exposition (ECCE)*, 2020: IEEE, pp. 1239-1243.

[15] S.-Y. Yu, C. Hsiao, and J. Weng, "A High Frequency CLLLC Bi-directional Series Resonant Converter DAB Using an Integrated PCB Winding Transformer," in *2020 IEEE Applied Power Electronics Conference and Exposition (APEC)*, 2020: IEEE, pp. 1074-1080.

[16] M. H. Ahmed, A. Nabih, F. C. Lee, and Q. Li, "Low-loss integrated inductor and transformer structure and application in regulated LLC converter for 48-V bus converter," *IEEE Journal of Emerging and Selected Topics in Power Electronics,* vol. 8, no. 1, pp. 589-600, 2019.

[17] W. Liu and J. Van Wyk, "Design of integrated LLCT module for LLC resonant converter," in *Twentieth Annual IEEE Applied Power Electronics Conference and Exposition, 2005. APEC 2005.*, 2005, vol. 1: IEEE, pp. 362-368.

[18] Y. Zhang, D. Xu, K. Mino, and K. Sasagawa, "1MHz-1kW LLC resonant converter with integrated magnetics," in *APEC 07-Twenty-Second Annual IEEE Applied Power Electronics Conference and Exposition*, 2007: IEEE, pp. 955-961.

[19] B. Li, Q. Li, and F. C. Lee, "High-frequency PCB winding transformer with integrated inductors for a bi-directional resonant converter," *IEEE Transactions on Power Electronics,* vol. 34, no. 7, pp. 6123-6135, 2018.

[20] S. De Simone, C. Adragna, and C. Spini, "Design guideline for magnetic integration in LLC resonant converters," in *2008 International Symposium on Power Electronics, Electrical Drives, Automation and Motion*, 2008: IEEE, pp. 950-957.

[21] Z. Ouyang, W. G. Hurley, and M. A. Andersen, "Improved Analysis and Modeling of Leakage Inductance for Planar Transformers," *IEEE Journal of Emerging and Selected Topics in Power Electronics,* vol. 7, no. 4, pp. 2225-2231, 2018.

[22] Z. Ouyang, J. Zhang, and W. G. Hurley, "Calculation of leakage inductance for high-frequency transformers," *IEEE Transactions on Power Electronics,* vol. 30, no. 10, pp. 5769-5775, 2014.

[23] Z. Ouyang, O. C. Thomsen, and M. A. Andersen, "The analysis and comparison of leakage inductance in different winding arrangements for planar transformer," in *2009 International Conference on Power Electronics and Drive Systems (PEDS)*, 2009: IEEE, pp. 1143-1148.

[24] M. Mu, L. Xue, D. Boroyevich, B. Hughes, and P. Mattavelli, "Design of integrated transformer and inductor for high frequency dual active bridge GaN Charger for PHEV," in *2015 ieee applied Power electronics conference and exposition (aPec)*, 2015: IEEE, pp. 579-585.

[25] B. Yang, R. Chen, and F. C. Lee, "Integrated magnetic for LLC resonant converter," in *APEC. Seventeenth Annual IEEE Applied Power Electronics Conference and Exposition (Cat. No. 02CH37335)*, 2002, vol. 1: IEEE, pp. 346-351.

[26] M. Meinhardt, M. Duffy, T. O'Donnell, S. O'Reilly, J. Flannery, and C. O. Mathuna, "New method for integration of resonant inductor and transformer-design, realisation, measurements," in *APEC'99. Fourteenth Annual Applied Power Electronics Conference and Exposition. 1999 Conference Proceedings (Cat. No. 99CH36285)*, 1999, vol. 2: IEEE, pp. 1168-1174.

[27] M. Li, Z. Ouyang, B. Zhao, and M. A. Andersen, "Analysis and modeling of integrated magnetics for LLC resonant converters," in *IECON 2017-43rd Annual Conference of the IEEE Industrial Electronics Society*, 2017: IEEE, pp. 834-839.

[28] J. Zhang, Z. Ouyang, M. C. Duffy, M. A. Andersen, and W. G. Hurley, "Leakage inductance calculation for planar transformers with a magnetic

shunt," *IEEE Transactions on Industry Applications,* vol. 50, no. 6, pp. 4107-4112, 2014.
[29] M. Li, Z. Ouyang, and M. A. Andersen, "High-frequency LLC resonant converter with magnetic shunt integrated planar transformer," *IEEE Transactions on Power Electronics,* vol. 34, no. 3, pp. 2405-2415, 2018.
[30] J. Hu and C. R. Sullivan, "The quasi-distributed gap technique for planar inductors: Design guidelines," in *IAS'97. Conference Record of the 1997 IEEE Industry Applications Conference Thirty-Second IAS Annual Meeting*, 1997, vol. 2: IEEE, pp. 1147-1152.
[31] J. Hu and C. R. Sullivan, "AC resistance of planar power inductors and the quasidistributed gap technique," *IEEE Transactions on Power Electronics,* vol. 16, no. 4, pp. 558-567, 2001.
[32] S. A. Ansari, J. N. Davidson, and M. P. Foster, "Analysis, Design and Modelling of Two Fully-Integrated Transformers with Segmental Magnetic Shunt for LLC Resonant Converters," in *IECON 2020 The 46th Annual Conference of the IEEE Industrial Electronics Society*, 2020: IEEE, pp. 1273-1278.
[33] S. De Simone, "LLC resonant half-bridge converter design guideline," *STMicroelectronics, Application Note AN2450,* p. 35, 2014.

Sajad A. Ansari was born in Shahrood, Iran, in 1994. He received the B.S. and M.S. degrees in electrical engineering from Shahrood University of Technology, Shahrood, Iran in 2016 and Amirkabir University of Technology, Tehran, Iran in 2019, respectively.
He is currently pursuing his PhD at the Department of Electronic and Electrical Engineering at The University of Sheffield, Sheffield, UK.
His research interests include renewable energy, and design and control of power electronic converters.

Jonathan N. Davidson received the M.Eng. degree in electronic engineering and the Ph.D. degree in thermal modelling and management from the University of Sheffield, Sheffield, U.K., in 2010 and 2015, respectively.
In 2015, he became a Lecturer in electrical engineering at the University of Sheffield. His research interests include thermal modelling and management of power electronics, and the design and analysis of piezoelectric transformer-based power converters, high-voltage power supplies for plasma chemistry and waste-water sensing systems.

Martin P. Foster received the B.Eng. degree in electronic and electrical engineering, the M.Sc.(Eng.) degree in control systems, and the Ph.D. degree for his thesis “Analysis and Design of High-order Resonant Power Converters” all the University of Sheffield, Sheffield, U.K., in 1998, 2000, and 2003, respectively. Since 2003, he has been a member of the academic staff in the Department of Electronic and Electrical Engineering, The University of Sheffield, where he is involved in power electronic systems. His current research interests include the modelling and control of switching power converters, resonant power supplies, multilevel converters, battery management, piezoelectric transformers, power electronic packaging, and autonomous aerospace vehicles.